Probing the extragalactic fast transient sky at minute time-scales with DECam

I. Andreoni [1,2,3,4]★ J. Cooke,[1,3,5] S. Webb,[1,3] A. Rest,[6,7] T. Pritchard,[1,8]
M. Caleb [1,9,10] S.-W. Chang [3,5,9] W. Farah,[1] A. Lien,[11,12] A. Möller [5,9]
M. E. Ravasio,[1,13,14] T. M. C. Abbott,[15] S. Bhandari,[1,16] A. Cucchiara,[17] C. Flynn,[1]
F. Jankowski [1,5,10] E. F. Keane [18] T. J. Moriya [19] C. A. Onken,[5,9]
A. Parthasarathy [1,3,16] D. C. Price,[1,20] E. Petroff [21,22] S. Ryder,[2,23] D. Vohl[22]
and C. Wolf [5,9]

Affiliations are listed at the end of the paper

ABSTRACT

Searches for optical transients are usually performed with a cadence of days to weeks, optimized for supernova discovery. The optical fast transient sky is still largely unexplored, with only a few surveys to date having placed meaningful constraints on the detection of extragalactic transients evolving at sub-hour time-scales. Here, we present the results of deep searches for dim, minute-time-scale extragalactic fast transients using the Dark Energy Camera, a core facility of our all-wavelength and all-messenger Deeper, Wider, Faster programme. We used continuous 20 s exposures to systematically probe time-scales down to 1.17 min at magnitude limits $g > 23$ (AB), detecting hundreds of transient and variable sources. Nine candidates passed our strict criteria on duration and non-stellarity, all of which could be classified as flare stars based on deep multiband imaging. Searches for fast radio burst and gamma-ray counterparts during simultaneous multifacility observations yielded no counterparts to the optical transients. Also, no long-term variability was detected with pre-imaging and follow-up observations using the SkyMapper optical telescope. We place upper limits for minute-time-scale fast optical transient rates for a range of depths and time-scales. Finally, we demonstrate that optical g-band light-curve behaviour alone cannot discriminate between confirmed extragalactic fast transients such as prompt GRB flashes and Galactic stellar flares.

Key words: stars: flare – gamma-ray burst: general – supernovae: general – radio continuum: transients.

1 INTRODUCTION

The optical transient sky is largely unexplored at short time-scales. Most successful time-domain surveys aim at detecting supernovae and variable events evolving on week or month time-scales. Those include, for example, the Supernova Legacy Survey (Astier et al. 2006), the Calán/Tololo Survey (Hamuy & Pinto 1999), the Palomar Transient Factory (PTF; Rau et al. 2009), the Catalina Sky Survey (Drake et al. 2009), Pan-STARRS (Stubbs et al. 2010), the Dark Energy Survey (DES; Dark Energy Survey Collaboration 2016), the All-Sky Automated Survey for Supernovae (ASAS-SN; Shappee

et al. 2014; Holoien et al. 2017), and now the Asteroid Terrestrial-impact Last Alert System (ATLAS[1]) and the Zwicky Transient Facility (ZTF;[2] Bellm et al. 2019; Graham et al. 2019) among others.

Recent work unveiled new classes of luminous, rapidly evolving supernovae (Kasliwal et al. 2010; Poznanski et al. 2010; Drout et al. 2014; Arcavi et al. 2016; Shivvers et al. 2016; De et al. 2018; Pursiainen et al. 2018; Rodney et al. 2018) performing observations with nightly and sub-nightly cadence. Rest et al. (2018) present the most extreme of these luminous fast transients discovered to date, which shows a rise time of 2.2 d, a time above half-maximum of

★ E-mail: igor.andreoni@gmail.com

[1] http://atlas.fallingstar.com/
[2] https://www.ztf.caltech.edu/

only 6.8 d, and a peak luminosity comparable to Type Ia supernovae. Bright optical flashes have also been observed during rapid follow up of long gamma-ray bursts using robotic telescopes (Fox et al. 2003; Cucchiara et al. 2011; Martin-Carrillo et al. 2014; Vestrand et al. 2014; Troja et al. 2017).

Rapid optical and infrared transients of high interest are kilonovae, which are associated with gravitational-wave events (e.g. Abbott et al. 2017) in addition to short gamma-ray bursts (Perley et al. 2009; Tanvir et al. 2013; Berger, Fong & Chornock 2013a; Gao et al. 2015; Jin et al. 2015, 2016; Troja et al. 2018; Jin et al. 2019). The discovery of a kilonova counterpart to the neutron-star merger GW170817 allowed the precise pin-pointing of the event in the sky (Arcavi et al. 2017; Coulter et al. 2017; Lipunov et al. 2017; Soares-Santos et al. 2017; Tanvir et al. 2017; Valenti et al. 2017) and allowed more than 70 facilities to monitor its evolution at many wavelengths (e.g. Abbott et al. 2017). Now we know that multiple components characterize the emission arising from mergers such as GW170817 (see e.g. Cowperthwaite et al. 2017; Kasliwal et al. 2017; Villar et al. 2017). In particular, observations of this transient revealed an early, blue component that evolves in about 3 d (with a rising phase of hours), but its origin is still unclear. Early detection and monitoring of a population of kilonovae can allow us to understand the nature of this rapidly evolving component (Arcavi 2018). As multimessenger astronomy grows in importance, more and more surveys are dedicated to the search for kilonova-like transients (e.g. Doctor et al. 2017) or to probe the background of contaminant sources during the follow up of gravitational-wave triggers (Cowperthwaite et al. 2018).

In addition to dedicated observing campaigns, new searches for fast optical transients are performed in archival data of surveys such as DES (Pursiainen et al.) and PTF (Ho et al. 2018). In the latter, the authors discovered an already-identified gamma-ray burst afterglow that was identified independently from gamma-ray triggers (Cenko et al. 2015). The Sky2Night project (van Roestel et al. 2019) searched for fast transients using PTF, with observations performed with 2 h cadence for eight nights. van Roestel et al. (2019) place upper limits on rates of 4 h and 1 d time-scale transients at $R < 19.7$ limiting magnitude, obtaining $R < 37 \times 10^{-4}\,\mathrm{deg}^{-2}\,\mathrm{d}^{-1}$ and $R < 9.3 \times 10^{-4}\,\mathrm{deg}^{-2}\,\mathrm{d}^{-1}$, respectively.

Only a few wide-field surveys have been carried out at time-scales shorter than 1 h. The continuous 30-min cadence of the *Kepler* K2 project led to the first discovery of the optical shock breakout of a core-collapse supernova (Garnavich et al. 2016, but see also Rubin & Gal-Yam (2017)). If considered independently from the long-lasting supernova emission, this constitutes a rare example of hour-time-scale extragalactic fast transient detection. Bersten et al. (2018) present the remarkable discovery of another optical supernova shock breakout, revealing an increase by $\Delta M_V \sim 0.6$ in ~ 25 min and estimated to last ~ 0.1 d. Other fast-cadenced surveys include a monitoring of the Fornax galaxy cluster (Rau et al. 2008), and blind surveys such as ROTSE III (Rykoff et al. 2005), the Deep Lens Survey (DLS; Becker et al. 2004), MASTER (Lipunov et al. 2007), and Pi of the Sky (Sokołowski et al. 2010). Results from the Pan-STARRS Medium-Deep Survey were reported by Berger et al. (2013b). The authors provided a summary of the upper limits on extragalactic fast optical transients evolving on ~ 0.5 h time-scales until 2013: the upper limits placed by all those surveys (Fig. 6) confirm that Galactic M-dwarf flares outnumber extragalactic fast transients by a large factor (up to several orders of magnitude; Rau et al. 2008). More recent surveys explore similar short-time-scale regimes, for example the High Cadence Transient Survey (HiTS; Förster et al. 2016). Interesting detections of fast-rising transients, increasing their luminosity by >1 mag in the rest-frame near-ultraviolet wavelengths between two consecutive nights (Tanaka et al. 2016), fuels the field of fast transient searches with exciting prospects.

Current surveys such as ZTF and Catalina Sky Survey can provide data suitable to search for minute- to hour-time-scale transients. In the near future, the Large Synoptic Survey Telescope (LSST; LSST Science Collaboration 2009) is expected to come online. LSST will survey the sky to deep magnitude limits and thanks to its large field of view ($\sim 10\,\mathrm{deg}^2$) it is expected to discover several thousands of extragalactic transients every night. The choice of the observing cadence will determine the degree to which LSST can contribute to different research areas in time domain astronomy.

This work aims to explore a new region of the optical luminosity-time-scale phase space (e.g. Cenko 2017), focusing on the search for faint extragalactic transients fully evolving in min. We performed deep and fast-cadenced observations with the Dark Energy Camera (DECam; Flaugher et al. 2015), a wide-field imager mounted at the prime focus of the 4 m Blanco telescope at the Cerro Tololo Inter-American Observatory (CTIO) in Chile. Such observations were performed in the framework of the Deeper Wider Faster programme[3] (Andreoni & Cooke 2018; Cooke et al., in preparation), described in the next section. Fast-cadenced observations with DECam are a key optical component of DWF that enables new studies, including the search for counterparts to fast radio bursts (FRBs; Lorimer et al. 2007) at many other wavelengths. FRBs are transients detected at radio wavelengths as dispersed signals that last only a few milliseconds. Several arguments support an extragalactic origin for FRBs, including the identification of the host galaxy of the repeating burst FRB 121102 (Tendulkar et al. 2017). However, the nature of FRBs is still unknown, thus the detection of possible optical or high-energy counterparts could shed light on the FRB physics.

A subset of the total quantity of optical data collected during DWF campaigns is analysed and presented in this paper (Tables 1 and 2). The chosen observations allow the most systematic analysis of minute-time-scale fast transients over multiple nights, as the observing conditions were the most uniform of the full data set.

The paper is organized as follows. Observations are presented in Section 2. Our analysis is described in Section 3 and its results are presented in Section 4. Searches for longer duration optical transients, FRBs, and GRBs are presented in Section 5. Rates for fast optical transients in the survey-depth transient-time-scale phase space are presented in Section 6. We discuss the results in Section 7 and we conclude with a summary of this work in Section 8.

2 OBSERVATIONS

We describe the Deeper Wider Faster programme in Section 2.1, the criteria driving the choice of the target fields in Section 2.2, and the characteristics of the unique, fast-cadenced optical images in Section 2.3.

2.1 The Deeper Wider Faster programme

The DWF programme is designed to unveil the fastest and most elusive bursts in the sky. Identifying counterparts to FRBs constitute the primary goal of the programme. The novelty of the approach adopted by the DWF team resides in coordinating deep, wide-field,

[3] http://dwfprogram.altervista.org/

Table 1. Equatorial (J2000) and Galactic coordinates of the target fields selected for this work, from a larger DWF data set.

Target field	RA	Dec.	l	b
3 h	03:00:00	−55:25:00	272.47784°	−53.43243°
4 h	04:10:00	−55:00:00	264.94437°	−44.75641°
Prime	05:55:07	−61:21:00	270.35527°	−30.26267°
FRB131104	06:44:00	−51:16:00	260.53726°	−21.94809°
Antlia	10:30:00	−35:20:00	272.94307°	−19.17249°

Table 2. Total time (expressed in hours) for which the target fields were observed.

Date YYMMDD	Target field 3 h	4 h	Prime	FRB131104	Antlia
151218	0.98	1.18	–	–	–
151219	1.21	1.24	–	–	–
151220	1.40	0.91	–	–	–
151221	1.47	1.05	–	–	–
151222	1.66	0.23	–	–	–
170202	–	–	0.97	0.96	0.86
170203	–	–	1.35	0.58	1.00
170205	–	–	1.11	0.87	0.72
170206	–	–	0.96	0.98	1.00
170207	–	–	1.03	1.02	1.02

fast-cadenced observations *simultaneously* with multiple small to large all-messenger facilities. By contrast, most of the existing efforts to accomplish the same science goals rely on different observing strategies. Usually when an interesting transient is detected by the survey telescope (or neutrino and gravitational-wave detectors), then a network of facilities receives the trigger and reacts to follow up the transient. Such a *reactive* approach has several limitations, for example the multiwavelength information is usually collected hours or days after the first detection. This causes the loss of possibly significant information or, in the case of FRBs, may be the cause of the lack of any counterpart discovered to date.[4] During DWF campaigns the fields are observed at multiple wavelengths in a *proactive* way: before, during, and after minute- and sub-minute-time-scale fast transients shine. Rapid detection and prompt and long-term follow up of transients is key to the success of the programme. Blanco/DECam has been the core optical facility during the first five DWF observing runs (2 pilot and 3 operational runs), spanning between 2015 January and 2017 February.

By 2018, the DWF programme has grown and now has more than 40 participating facilities, including the Subaru/Hyper Suprime-Cam (HSC) used as the core optical instrument for simultaneous observations in 2018 February 2018. The thorough analysis of the Subaru and the multiwavelength data will be presented in future publications.

2.2 Target fields

Coordinating multiple telescopes that shadow each other constrains the region of sky observable during simultaneous observations. Such limitations become particularly significant when the observatories are located on different continents. In fact, the ground-based core facilities used during DWF from 2015 to 2017 for simultaneous or rapid follow-up observations are located in Chile (Blanco/DECam, Rapid Eye Mount telescope, Gemini-South) and in Australia (Parkes, Molonglo, ATCA, and SkyMapper). Constraints change when using core facilities other than DECam and Australian radio telescopes for DWF observations, for example when using Subaru/HSC in Hawaii, or the MeerKAT radio telescope in South Africa in the near future. For space-based observatories such as *Swift*, constraints include limited time on fields far from the poles, Earth occultation times, and Sun constraints.

We demonstrated that these specific geographical constraints can be overcome (Cooke et al., in preparation) and successful DWF

[4]Hardy et al. (2017) report upper limits on optical flux at times coincident with bursts from the repeating FRB 121102. The extremely fast cadence of Thai National Telescope/ULTRASPEC (70.7 ms frames) makes their results meaningful, however we caution that (i) possible optical emission could have been fainter than the 5σ upper limit of ULTRASPEC ($m_i \sim 15.75$, AB) and (ii) FRB 121102 may not be representative of the whole FRB population.

observations from Chile and Australia can be performed all year around. We chose the target fields in relation to the following criteria:

(i) Sky locations where FRBs were previously discovered (here FRB131104). The field of view of the 13-beam receiver at Parkes (see Section 5.2) well matches the DECam field of view (FoV) but, in addition, the localization error for those FRBs discovered with Parkes ($\sim$15 arcmin diameter) allows targeted, simultaneous observations using telescopes with FoV smaller than DECam, such as REM and *Swift*/UVOT-XRT.

(ii) Nearby galaxy clusters (e.g. Antlia), nearby galaxies, or globular clusters.

(iii) Legacy fields (e.g. COSMOS field) having dense photometric and spectroscopic information in multiple wavelengths and space-based high-resolution imaging; and/or fields where we have previous DECam deep imaging and colour information, located at high Galactic latitude and observable for $\gtrsim$1 h from Chile and Australia (Prime, 3 h, 4 h).

More than 15 fields were observed with high-cadence simultaneous observations during DWF observing runs. Table 1 reports the coordinates of target fields whose data are analysed in this work.

2.3 Fast-cadence imaging with DECam

DWF observing campaigns have produced a large quantity of multiwavelength data. These are analysed in real time or near-real time to search for FRBs, their possible counterparts, and to discover Galactic and extragalactic fast transients. DWF collected $\gtrsim$ 10 000 optical images with DECam, mainly in the g filter, which allows $\sim$0.5 mag deeper observations in comparison with other filters. The expected depth for 20 s exposure in g-band is 23.7 mag (AB), against 22.6, 23.1, 22.6, and 21.6 mag of the u–r–i–z filters, respectively (1.0 arcsec FWHM seeing). Typical seeing and relatively high airmass ($\sim$1.5) required for the coordinated observations can affect these values, sometimes moving the g-band limiting magnitude closer to $\sim$23 mag.

The observing strategy with DECam during DWF runs is based on a series of continuous exposures. Our experience has shown that a 20 s exposure time is optimal to (1) enable sub-minute-time-scale variability exploration, (2) reach individual image depth $\geq$23 to observe large sky volumes, (3) enable efficient data transfer and image subtraction in real time, and (4) probe a range of depths and durations when images are analysed individually and in various stacked forms.
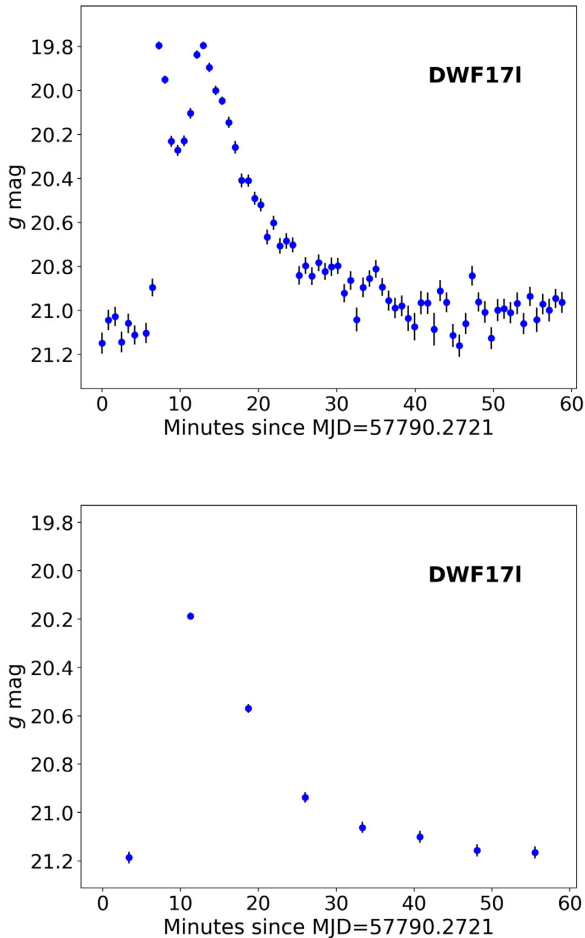
Figure 1. The multipeak structure of DWF17l is visible in light curves built with series of 20 s exposure images (top panel), but is lost when stacking sets of nine images (bottom panel). Even if some time resolution is lost, stacking of images acquired during DWF observations allows deeper and more fast-cadenced searches than most existing surveys. The source DWF17l is located at coordinates RA = 6:42:20.333, Dec. = –52:10:24.78 (J2000) and the colour of its quiescent counterpart suggests the flare to have arisen from an M5 red-dwarf star.

Telescope movements are limited to a few arcseconds in order to cover the largest common area of the sky with adjacent exposures. In this work, we analyse 25.76 h of high-cadenced images: 20 s continuous exposures in *g* band, separated by ∼30 s where CCDs complete the readout and the new exposures start. Each image covers an effective field of view of 2.52 deg^2, accounting for CCD gaps and the frame area cropped during the alignment of the images. Details of the observations discussed in this work are presented in Table 2. Data are processed and calibrated with the NOAO High-Performance Pipeline System (Swaters & Valdes 2007; Valdes & Swaters 2007)

The high cadence of our images allows us to study transient and variable events in great detail. For example, the structure of the stellar flare DWF17l in Fig. 1, sampled at 50 s intervals (20 s exposure + 30 s overhead), is lost when median-stacking sets of nine consecutive images, equating to ∼7 min intervals. Similarly, fast-cadence imaging reveals a non-monotonic fade of the light curve of DWF17ax, difficult to study at slower cadence (Fig. 2).
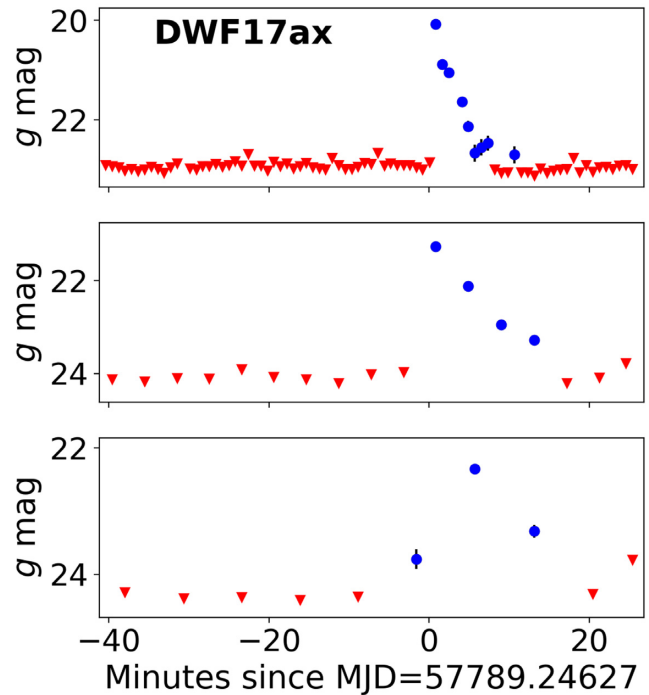

Figure 2. Light curves of the fast transient candidate labelled DWF17ax (whose discovery images are shown in Fig. 3) obtained with individual 20 s exposures (*top*) and by stacking sets of five (*centre*) and nine (*bottom*) fast-cadence images. Red triangles indicate 5σ upper limits.
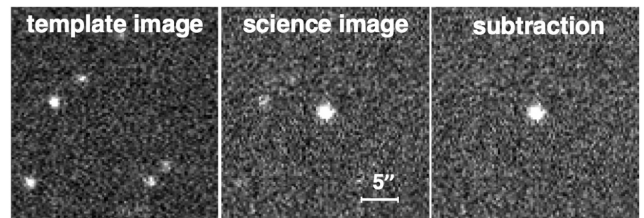

Figure 3. Example of detection 'postage-stamp' images. The eFTC (in this case DWF17ax) is present in the science image (*centre*) and is not present at the same coordinates in the deeper template images (*left*). The image subtraction between science and template images leaves a bright, PSF-shaped residual brighter than the background (*right*). The light curve of DWF17ax is shown in Fig. 2.

3 ANALYSIS: SEARCH FOR EXTRAGALACTIC FAST TRANSIENT CANDIDATES

Data are searched using the custom *Mary* pipeline (Andreoni et al. 2017). The pipeline identifies optical transients with image subtraction techniques, processing all CCDs in parallel with the Green II (g2) supercomputer at Swinburne University of Technology (now superseded by the OzStar supercomputer).

The *Mary* pipeline automatically outputs a list of candidates and generates three small 'postage-stamp' images for each candidate for visual inspection (see e.g. Fig. 3). In addition, a companion code generates aperture photometry light curves centred at the location of the discoveries, with radius 1.5 × FWHM measured from nearby stars. Light curves presented in this paper are first calibrated against the all-sky USNO-B1 catalogue (which provides a number

of Southern hemisphere sources large enough to enable calibration of individual CCDs independently) and then calibrated against the AAVSO Photometric All Sky Survey (APASS; Henden et al. 2016) catalogue that provides AB system measurements. Our tests indicated the *g*-band magnitudes obtained this way to be consistent with magnitudes from the Sloan Digital Sky Survey catalogue (where there is overlap with DWF fields) within $\lesssim 0.1$ mag.

Template images used for the analysis are always deeper than the individual 20 s exposure images, however their limiting magnitude is usually different for different fields, depending on the availability of archival images from previous observations. For the identification of short-time-scale optical transients it is not necessary to have template images older than a few minutes, however the availability of deep templates obtained ad much earlier/later times can greatly help the classification process. When fast transients are identified, we perform a more accurate classification of the detections, based on the photometry performed on deep images, multifilter information, and object information found when cross-matching with existing catalogues. Asteroids are easily identifiable thanks to the fast cadence of the observations, which makes the movement of the objects in the sky evident when comparing a chronological sequence of images.

First, we search for transient and variable sources in 1870 individual 20 s-exposure images, taken with regular cadence. Secondly, we stack the images in sets of 5, 9, 13, and 17 images to reach deeper magnitude limits and search for fainter fast-evolving transients.

3.1 Selection criteria

At the end of the processing, candidates automatically identified with the *Mary* pipeline are selected aiming at identifying extragalactic fast transient candidates (eFTCs). In particular, we search for astrophysical transient events that evolve at minutes time-scales and are not spatially coincident with Galactic sources.

When searching for eFTCs we consider only the first night that a detection occurs for those objects detected in more than one night. Upon first detection of a luminosity increase (using image subtraction) at a certain sky location, the pipeline assigns a running ID number to the sky coordinates of the detected object. Consequently, possible re-brightening of the source in the following nights is not given a new ID number and it is not considered among fast transient candidates presented in this paper.

Our searches returned a large number of candidates ($> 600\,000$) most of which are spurious detections, transient/variable objects evolving at long time-scales, or Galactic in origin. We reduce the number of spurious detections by requiring candidates to be detected ≥ 2 consecutive times. Further selection criteria include constraints on the duration of the transients and the rejection of those likely of Galactic origin.

We excluded those events detected at the beginning and/or at the end of each night, constraining the maximum evolution time-scales within the time spent on a target field on each night, typically ~ 1 h (Table 2). An example of a transient rejected from our sample because it was detected too close to the end of the night is provided in Fig. 4.

Searching separately for transients evolving at different time-scales (e.g. 2 min against 20 min full-evolution time) brings several advantages. For example, it enables the rejection of Galactic sources that emit rapid outbursts such as dwarf novae and some active M-dwarfs, favouring the identification of individual minute-time-scale bursts. We enhanced the completeness of our searches by allowing the pipeline to 'miss' a number of detections (termed
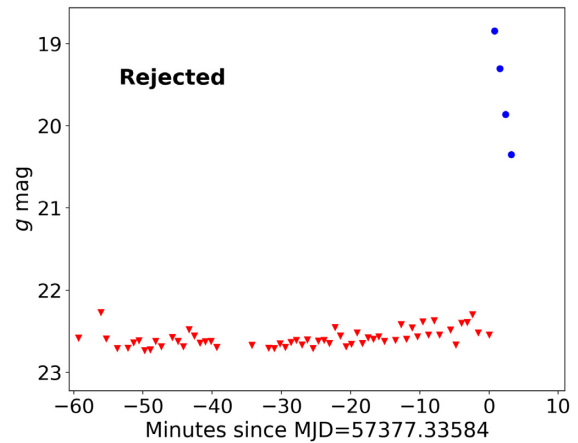

Figure 4. Light curve of an eFTC that did not fulfil the selection criteria described in Section 3. In particular, the candidate was detected in the last image acquired on the observing night in which it was discovered, but we require at least one epoch of non-detection at the beginning and at the end of each observing night to better constrain the transient duration.

Table 3. Criteria used for the transient selection. Each row represents a search criterion adopted for each field for each observing night. The first column presents the minimum number of times that a candidate was detected by the *Mary* pipeline; the second column presents the maximum number of images between the first and last detections of each candidate on a given night (extremes included); the third column shows the maximum number of non-detections ('holes') allowed between the first and last detection; the last column indicates the minimum number of 'empty' images, both at the beginning and at the end of each given night, in which the candidate must *not* be detected in order to pass the selection.

Min det	Max det	Holes	Empty
2	2	0	1
3	5	1	2
6	8	2	2
9	11	3	2
12	16	4	2
17	23	6	2
24	32	8	2
33	47	12	2
48	64	16	2

'holes') between the first and the last detection of a candidate, on the night of first detection. We chose the ratio between the number of holes and the minimum number of detections to be $\sim 1/3$. Table 3 summarizes the number of holes that we allowed to be present for each time-scale, constrained between the minimum and maximum number of detections. Fig. 5 helps visualize the selection criteria on the transient duration.

As we aim at identifying extragalactic fast transients, we introduced selection criteria to reduce the number of Galactic contaminants (variable and flare stars) in the sample. Using the Source Extractor (SEXTRACTOR, Bertin & Arnouts 2010) software on *g*-band stacks, we exclude those sources with a counterpart detected within a 2.2 arcsec radius with a star/galaxy classification
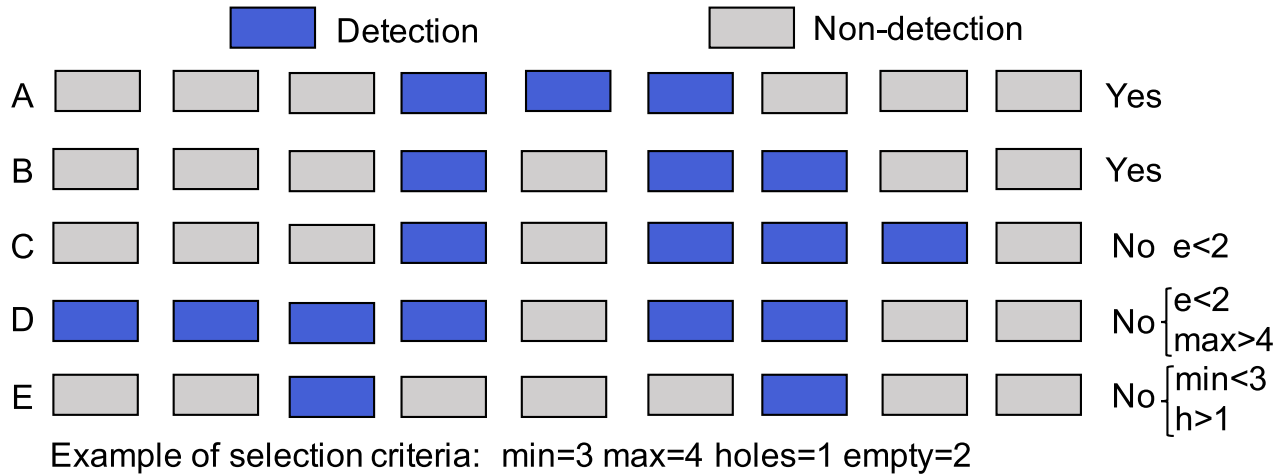
Figure 5. Example of selection criteria application. Given a set of consecutive images (nine images in this example, but of the order of hundred images per night during DWF observations), we define the following selection criteria: at least three detections (min = 3), at least two images without detection at the beginning and at the end of the observing night of that target field (empty = 2), at most four detections (max = 4), and at most one image without detection between the first and last detection (holes = 1). We apply up to nine collections of such selection criteria for each set of images in order to keep a nearly constant ratio of minimum number of detections and holes (see Table 3).

value CLASS_STAR > 0.95. Such a threshold accommodates the change in point spread function (PSF) across the large field of view of DECam and is conservative because it is more likely that stars are classified as galaxies than vice versa. Bleem et al. (2015) calculated that a CLASS_STAR threshold of 0.95 is expected to include 94 per cent of all possible galaxies in the field and excludes 95 per cent of all stars. First, we use CLASS_STAR to reduce the number of bright false positives without significant probability of missing true extragalactic sources, other than quasi-stellar objects (QSOs). Then, we use the SPREAD_MODEL parameter (computationally more expensive than CLASS_STAR) to improve the classification of those sources that survived our selection (Tables 4 and 5). The SPREAD_MODEL value does not depend directly on the S/N of the source, so it can separate stars from galaxies more effectively than CLASS_STAR close to the detection limit (see e.g. Sevilla-Noarbe et al. 2018). According to Annunziatella et al. (2013), a threshold of 0.005 provides an optimal compromise between a reliable classification and a low contamination, with sources with SPREAD_MODEL < 0.005 being likely stellar.

3.2 Stacking multiple images

In Section 2.3, we explained how we explored a data set made of a large number of 20 s exposures acquired with regular cadence. The exploration of the shortest time-scale dictated by the cadence returns one point in the 3D space defined by time-scale, depth, and areal rate (see Fig. 6 and Berger et al. 2013b). Assuming a constant limiting magnitude for each set of images, it is possible to search for transients exploring several time-scales, potentially from less than the exposure time up to the duration of the observation of the target field, thus obtaining an array of areal rates that, if well sampled, defines a broken line in Fig. 6.

We enrich the exploration of the parameter space of interest by dividing the images taken on each night in sets of 5, 9, 13, and 17 frames to be stacked together. The larger the number of images stacked together, the deeper we can search and therefore explore a bigger volume of Universe and detect fainter transients. This comes at the cost of reducing the temporal resolution and increasing the time-scales of the transients to be discovered, losing

information on their evolution, and reducing the effective areal exposure (see Section 6) given the finite total number of images available. The systematic exploration of pairs of time-scale and limiting magnitudes defines a surface in Fig. 6.

The criteria to select eFTCs in series of stacked images are the same as described in Section 3.1 and in Fig. 3, with the sole difference that the minimum number of 'empty' stacked images, both at the beginning and at the end of each given night, in which the candidate must not be detected in order to pass the selection is always equal to 1. The choice of the number of images to stack (1, 5, 9, 13, 17) and the type of stacking (median) are dictated by technical reasons. Stacking more than 17 images together would cause the analysis to be meaningless in several cases, as no transient would possibly meet the criteria for the selection. We found that considering steps of four images balances well the need to densely sample the exploration space and the availability of computational resources, highly demanded when running the pipelines on thousands of images. Moreover, stacking an odd number of images is particularly suitable for median-stacking. The limitation to stack images considering median values derives from the structure of the *Mary* pipeline used to perform the analysis, which lacks a cosmic ray-rejection module that reduces the number of false positives when stacking a large number of images using averaging. In fact, average-stacking would have allowed us to be more sensitive to bright events with very short duration, thus we acknowledge that average-stacking would have been the preferred choice to adopt in this work. We are planning to adopt average-stacking in future work. Nevertheless, median-stacking images allowed us to achieve excellent results.

4 RESULTS

In order to carry out the searches described in Section 3, we ran the *Mary* pipeline 2744 times in total, each time processing 59 CCDs in parallel. The analysis of our data set returned 318 672 candidates,[5]

---

[5]This number includes possible repetitions of the same candidate when stacking different sets of multiple images.

Table 4. Identification name, target field, and coordinates of those fast transient candidates that passed our selection criteria. The magnitude variation is computed as the difference between the deepest *g*-band measurement available and the observed peak magnitude therefore the actual variation in magnitude is likely larger than what is reported here. The light curves of the eFTC presented here are shown in Fig. 2 and in Figs 8 and 9. Candidates in the lower half of the table, below the horizontal line, are those for which CLASS_STAR alone on the multiband data cannot determine whether the quiescent counterpart to the transients is stellar.

ID	Field	RA	Dec.	$-\Delta g$	g	r	i	z
DWF15a	4 h	4:11:05.702	$-55{:}40{:}17.87$	~ 5.0	24.78 ± 0.20	23.86 ± 0.21	21.53 ± 0.08	–
DWF17a	Antlia	10:25:53.642	$-35{:}31{:}20.67$	>2.4	>24.15	23.64 ± 0.18	20.37 ± 0.01	19.90 ± 0.023
DWF17c	Antlia	10:28:48.603	$-36{:}07{:}00.54$	>2.4	>24.15	23.29 ± 0.12	21.09 ± 0.02	20.97 ± 0.07
DWF17f	Antlia	10:27:36.287	$-35{:}36{:}59.79$	1.8	23.53 ± 0.15	21.74 ± 0.04	18.96 ± 0.01	18.97 ± 0.01
DWF17g	Antlia	10:25:47.560	$-35{:}41{:}54.92$	0.8	21.61 ± 0.04	20.00 ± 0.01	18.198 ± 0.003	17.990 ± 0.005
DWF17k	FRB131104	6:47:05.788	$-51{:}27{:}38.88$	~ 4.8	25.19 ± 0.25	23.19 ± 0.11	20.50 ± 0.07	–
DWF17x	FRB131104	6:45:04.601	$-51{:}38{:}18.26$	>4.6	>25.0	>24.3	21.29 ± 0.26	–
DWF17ao	Prime	5:52:29.591	$-60{:}49{:}50.92$	3.6	25.46 ± 0.18	23.66 ± 0.10	21.86 ± 0.05	21.16 ± 0.01
DWF17ax	Prime	5:59:00.662	$-62{:}02{:}11.03$	>5.6	>25.6	24.53 ± 0.16	22.64 ± 0.09	21.98 ± 0.02

Table 5. SExtractor star/galaxy classification of short-listed eFTCs in quiescence in deep images using the CLASS_STAR (C_S) and the SPREAD_MODEL (S_M) parameters. The last column indicates whether the sources were classified as stellar with score S/G >0.95 in at least one band. In such cases, we consider the SExtractor classification to be in support of the eFTCs being Galactic stellar flares.

ID	C_S	S_M	C_S	S_M	C_S	S_M	C_S	S_M	S
	g	g	r	r	i	i	z	z	
DWF15a	0.59	0.0001 ± 0.0093	0.22	-0.0019 ± 0.0054	0.97	-0.0012 ± 0.0023	None	None	Y
DWF17a	None	None	0.01	0.0069 ± 0.0055	0.98	-0.0002 ± 0.0005	0.97	-0.0000 ± 0.0006	Y
DWF17c	None	None	0.74	-0.0027 ± 0.0038	0.98	0.0002 ± 0.0009	0.96	-0.0004 ± 0.0014	Y
DWF17f	0.55	-0.0095 ± 0.0046	0.98	0.0001 ± 0.0010	0.99	-0.0002 ± 0.0002	0.99	-0.0012 ± 0.0003	Y
DWF17g	0.72	0.0032 ± 0.0011	0.98	0.0039 ± 0.0003	0.98	0.0050 ± 0.0001	0.98	0.0052 ± 0.0002	Y
DWF17k	0.04	None	0.00	-0.0017 ± 0.0033	0.04	0.0006 ± 0.0009	None	None	Y
DWF17x	None	None	None	None	0.36	-0.0092 ± 0.0061	None	None	Y
DWF17ao	0.00	None	0.83	-0.0043 ± 0.0037	0.67	0.0005 ± 0.0006	0.85	-0.0002 ± 0.0004	Y
DWF17ax	None	None	0.00	0.0038 ± 0.0083	0.00	0.0003 ± 0.0012	0.33	-0.0007 ± 0.0006	Y

including thousands of real variable and transient sources along with a large number of false positives. We reduced the number of candidates to ∼10 000 by applying the selection criteria on the duration of the transients, presented in Table 3. All candidates were visually inspected at this preliminary stage and further inspection was performed after applying the following cuts.

When all the selection process described in Section 3.1 was completed, 1846 candidates remained. Visual inspection of those candidates, exclusion of asteroids, and the removal of repetitions due to the detection of the same object when stacking different sets of images left us with 25 candidates. Of those 25 candidates, we classified 1 as AGN activity, 2 were already catalogued as variable stars in the VizieR data base,[6] and 13 have parallax or high proper-motion measurements reported in the second *Gaia* Data Release (Gaia Collaboration 2016, 2018). Excluding those Galactic and nuclear sources from our sample, 9 eFTCs constitute our short list. Their identifications and sky coordinates are presented in Table 4. We stress that many more real transient sources were identified than those reported in this paper, however a limited number of those passed the selection criteria that we established.

We further investigate the colour information (Fig. 7) and behaviour of the light curves (Fig. 8-10) of the nine short-listed eFTCs using SExtractor CLASS_STAR and SPREAD_MODEL on deep stacks in *riz* bands (where available). Results of the multiband S/G classification are presented in Table 5. Five eFTCs (DWF15a, DWF17a, DWF17c, DWF17f, and
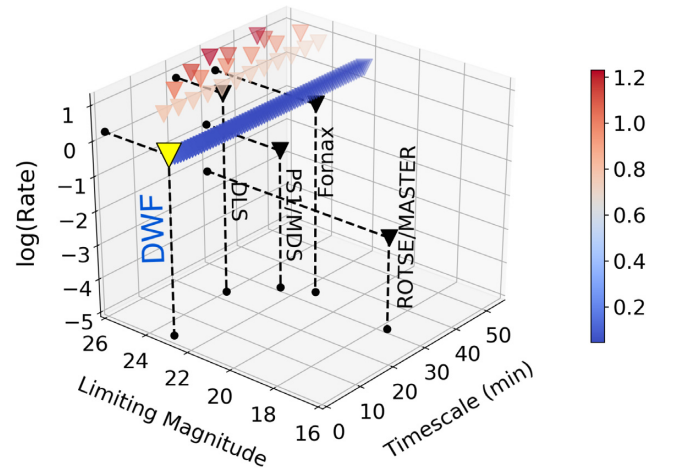
[6]https://vizier.u-strasbg.fr/viz-bin/VizieR

Figure 6. Plot of the new phase-space region explored, where rates of extragalactic fast transients (deg^{-2} d^{-1}) are plotted at each combination of limiting magnitude (i.e. depth) and time-scale (expressed in minutes). The colour-map also represents the logarithm of the rates and helps visualizing the differences between different points. Triangles indicate upper limits placed during the systematic exploration of the DWF data set presented in this paper, assuming that all the eFTCs that passed our selection criteria are Galactic or spurious detections. The stacking of sets of images allows the exploration of different depth regimes, thus our results approximately describe a surface in the limiting magnitude – time-scale – transient rates phase space. The yellow triangle represents the shortest time-scale that we can explore ($\tau = 1.17$ min), for which we obtain $R_{\text{eFT}} < 1.625$ deg^{-2} d^{-1}. Black triangles indicate upper limits for past surveys, here presented as in Berger et al. (2013b).
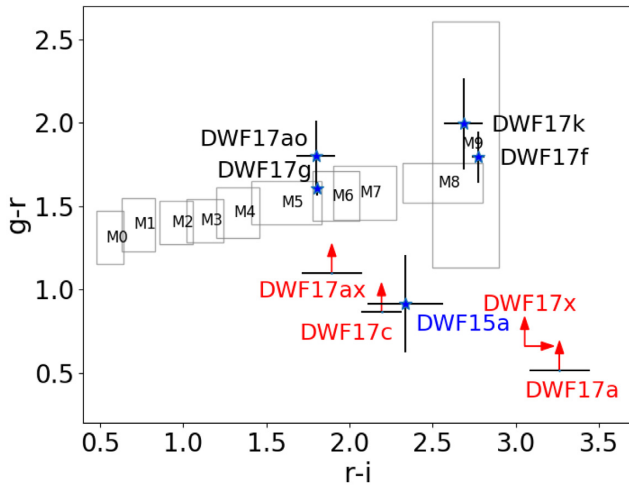
Figure 7. Colour–colour plot showing measurements of possible counterparts to the eFTCs listed in Table 4. Magnitude values were calibrated using the APASS catalogue. Boxes frame regions of the colour-colour plot where different types of M-dwarfs lie (West et al. 2011).

DWF17g) can be classified as stellar if we consider again an S/G threshold CLASS_STAR > 0.95. All nine sources are likely stellar considering the SPREAD_MODEL parameter, since SPREAD_MODEL < 0.005 in at least one band in all cases. Colours are obtained with photometric measurements on deep stacks of images acquired before the transient detection. Magnitudes are calibrated using the APASS (Henden et al. 2016) catalogue. Sources with a detectable counterpart in deep stacks and in different filters are plotted in Fig. 7 (see also Table 4). We also attempt a comparison between our data with flare-star models computed from *Kepler* observations (Davenport et al. 2014). One example of such a comparison is presented in Fig. 10 for the eFTC candidate DWF17a. The selected eFTCs are individually discussed below. As mentioned above, all these candidates are likely stellar based on the multiband S/G classification.

(i) DWF15a – Faint detections of the source in deep stacks place it outside the M-dwarf stripe in the $g - r, r - i$ colour plot. The light curve is consistent with a template flare-star light curve (Fig. 10).

(ii) DWF17a – The light curve evolves faster than the stellar flare model (Davenport et al. 2014) shown in (Fig. 10) We note that a large difference $r - i > 3$ suggests the flare to be generated from a star of type later than M9.

(iii) DWF17c, DWF17f – The light curves compare well with the stellar flare model. These sources can be classified as M7 (DWF17c) and M8-M9 (DWF17f) stellar flares.

(iv) DWF17g – Very likely M5–M6 star flare.

(v) DWF17k – The location in the colour–colour plot suggests DWF17k could be an M8–M9 star flare. A Galactic nature of this source is also supported by a good resemblance between the light curve and the template stellar flare we consider.

(vi) DWF17x – The upper limits in the colour–colour plot in Fig. 7 give little information about the nature of DWF17x. The light curve matches well the flare-star model (Fig. 10). The small discrepancy could be due to the wrong choice of the peak time that a higher cadence would have improved.

(vii) DWF17ao – The multipeak light curve advocates for a flare-star event that, according to the colour–colour plot in Fig. 7, may have an M5–M6 star progenitor.

(viii) DWF17ax – The fast-cadence light curve of DWF17ax (Fig. 2, top-left panel) shows a possible multipeak structure, common among flare stars. If the transient is indeed a flare star, its progenitor's class could range between M5 and M7.

5 SEARCHES FOR MULTIWAVELENGTH COUNTERPARTS

The DWF programme coordinates simultaneous multiwavelength observations of the target fields. Moreover, we take templates using the wide-field SkyMapper telescope weeks before DWF observing runs and we use it to perform interleaved, nightly observations during DWF, and late-time regularly cadenced observations weeks after DWF to characterize long-duration transients. In this section, we present searches for gamma-ray and radio signals possibly associated with the eFTCs that we selected using the Parkes, Molonglo, *Swift*, and *Fermi* observatries. While large data sets were analysed, particular attention was given to those eFTCs for which the S/G separation is less robust because it relies on the SPREAD_MODEL parameter only, instead of on both SPREAD_MODEL and CLASS_STAR parameters. Details and results of these searches are summarized in Table 6. Searches for long-duration optical transient counterparts with SkyMapper are described in Section 5.3.

5.1 Searches for gamma-ray signals

We explore data acquired with *Fermi* and *Swift* gamma-ray telescopes at times close to the last non-detection of our selected eFTC.

Neil Gehrels Swift Observatory

Observations with the *Neil Gehrels Swift Observatory* (hereafter *Swift*) were performed under approved Cycle 11 and Cycle 13 programmes (PI Pritchard). Moreover, the large FoV of *Swift*/Burst Alert Telescope (BAT; Barthelmy et al. 2005) allowed DWF target fields to be observed even when the satellite was pointing at other scientific programme targets with its narrower-field instruments X-ray Telescope (XRT) and UltraViolet/Optical Telescope (UVOT). The *Swift* team smartly scheduled *Swift* observations of other science programmes to maximize the observability of DWF fields with BAT. We searched for gamma-ray counterparts to five most promising eFTCs in particular: DWF15a, DWF17k, DWF17x, DWF17ao, DWF17ax. Some of the DWF *Swift* time had BAT, XRT, and UVOT on the target fields. However, none of the sources were located within the FoV of the XRT and UVOT therefore we limit our analysis to the BAT data.

We considered the last optical non-detection as onset time (T0). Onset times are listed in Table 6. We expect T0 to be accurate within 30 s from the actual onset of the eFTCs because of the short rise-time of the transients and the high cadence of our observations. The nature of the eFTCs being uncertain, we explored a conservative time window of ±1800 s around T0, larger than the evolution time-scale of the candidates. Except DWF17ao, all candidates were located in the BAT FoV for some period of time within the search interval. DWF17ao occurred when *Swift* was in safehold, so no data were available. A wider temporal search (years before and after the events) is planned for future work.

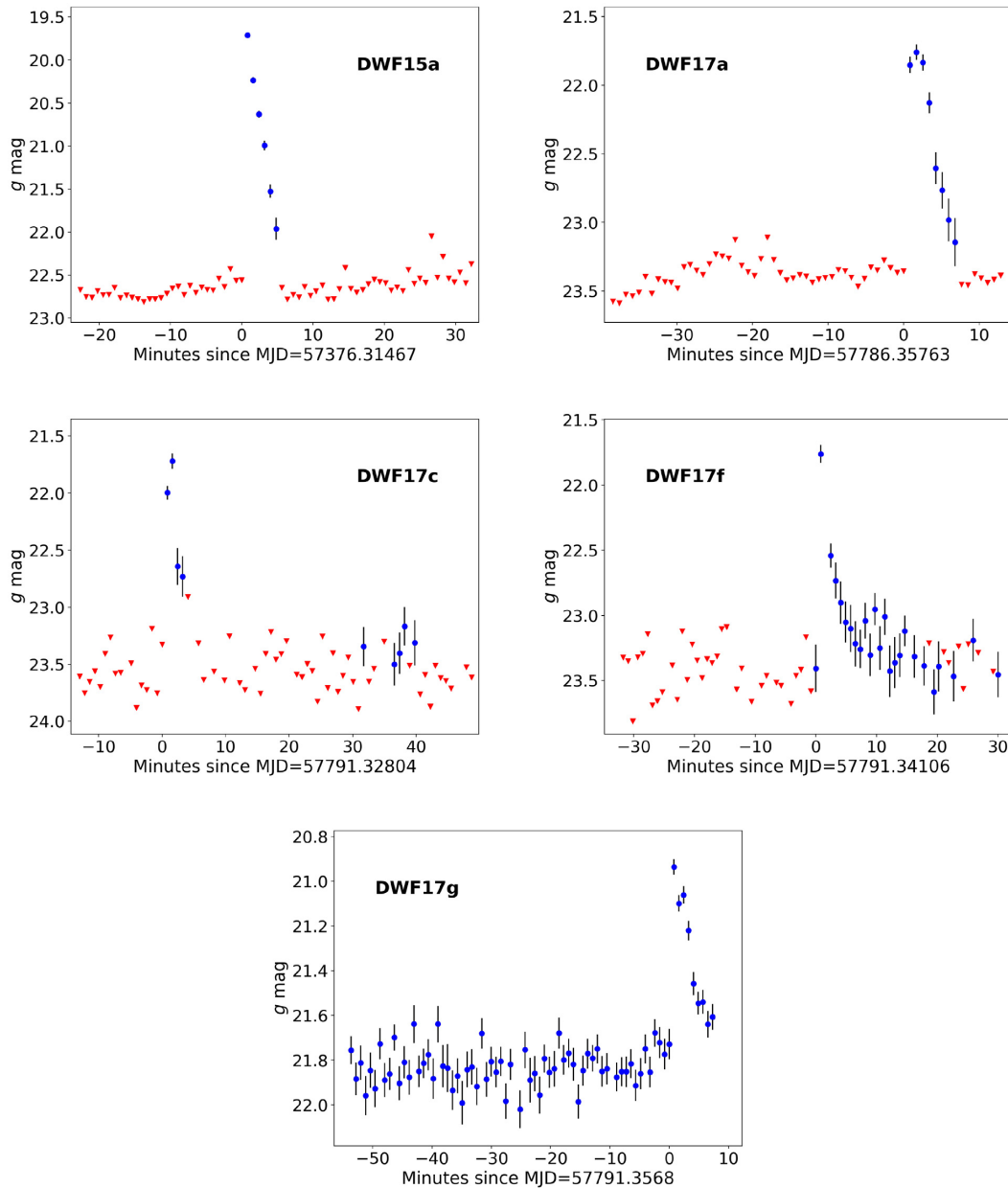When trying to identify gamma-ray counterparts, unconstrained by physical models, we searched:

Figure 8. Light curves of selected eFTCs that we classify as stellar flares based on the multiband S/G separation with both CLASS_STAR and SPREAD_MODEL (Table 5). Red triangles represent 5σ forced-photometry upper limits. Candidates DWF17f and DWF17g show measurements on the last epochs of the observing sequence, missed by the image-subtraction pipeline with threshold at $\sim 7\sigma$ significance. Details about these sources are presented in Table 4.

(i) The raw light curves, to see if there are any obvious GRB-like structures around T0. We did not find GRB-like events in raw light curves.

(ii) The available event data, from which we can make a background-subtracted (i.e. mask-weighted) light curve using the source location. In particular, we looked for astrophysical signals in mask-weighted light curves (e.g. burst-like features or some continuous time bins with count rate above $\sim 3\sigma$). We also created images of the available event data interval and search for any detections at the source location. No source was found above 3σ significance.

(iii) The BAT survey data, which consisted of continuous data binned in 300 s bins. Again, no signal was detected at the source locations at $>3\sigma$ significance.

In summary, no significant ($\gtrsim 3\sigma$) gamma-ray source was found when searching in BAT raw data, BAT event data, and BAT survey data within T0 $\pm$ 1800 s, where T0 is the onset time. More precise time slots in which the selected eFTCs were in the BAT FoV are reported in Table 6.

Fermi

We searched for GRB counterparts detected by the *Fermi* Gamma-ray Burst Monitor (GBM; Meegan et al. 2009) during the optical transients presented in this work. The GBM is composed of 12 sodium iodide (NaI) and two bismuth germanate (BGO) scintillation detectors, covering, respectively, the energy range 8 keV–1 MeV
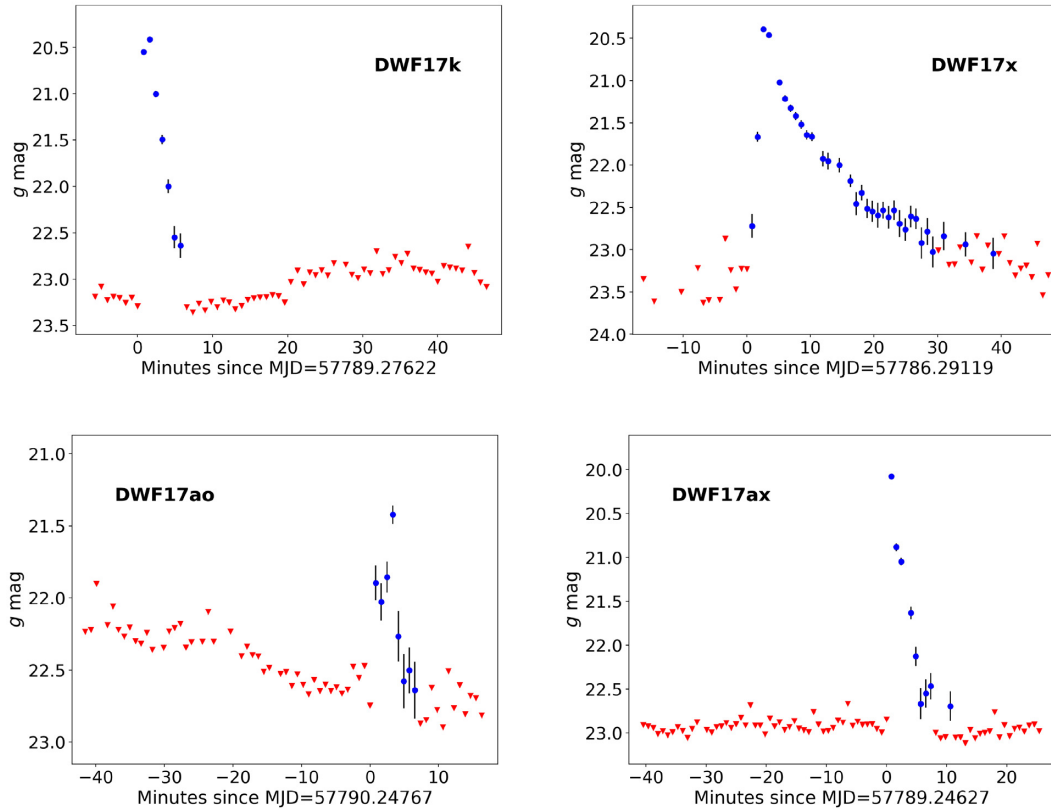
Figure 9. Light curves of selected eFTCs that we cannot classify as stellar flares based on CLASS_STAR, but that likely have stellar progenitors based on SPREAD_MODEL information. Details about the eFTCs are presented in Table 4. The light curve of DWF17ax can be found also in Fig. 2, where we show the effect of image stacking on a transient light curve.

and 200 keV–40 MeV, with a field of view >8 sr. We searched for counterparts in the Fermi GBM Burst Catalog,[7] that lists all triggers observed that have been classified as GRBs. For completeness, we also searched in the *Fermi* GBM Trigger Catalog,[8] that lists all triggers (even not classified as GRBs) observed by one or more of the 14 GBM detectors, and also in the Subthreshold Catalog.[9]

Table 6 reports the results of the research in the catalogues, with a time window of ± 1 d from the onset of the optical transient. No gamma-ray sources were found spatially and temporally coincident with the 10 optical transient reported in Table 4. However, we found three transients, DWF17c, DWF17f, and DWF17g, spatially located within the 3σ contour plot of the GBM localization of a GRB (GRB170208). This GBM event occurred on 2017 February 8 at 18:11:16.397, more than 1 d after the optical transients, and is separated by more than 10 degrees from the positions of the optical transients. Due to the time-lag between the optical and gamma-ray events and to the poor localization of the GBM detectors, we conclude that GRB170208 cannot be the counterpart to DWF17c, DWF17f, or DWF17g.

5.2 Searches for coincident fast radio bursts

Parkes – As part of the SUrvey for Pulsars and Extragalactic Radio Bursts (SUPERB) (Keane et al. 2018), we explored the data acquired

using the 21 cm multibeam receiver (Staveley-Smith et al. 1996) deployed on the Parkes radio telescope. The FWHM of each of the 13 beams is ~ 14 arcmin, with an areal $\sim 2\sigma$ 13-beam coverage of ~ 3 deg^2.

The output of each beam was processed by the Berkeley–Parkes–Swinburne Recorder (BPSR) mode of the HI-Pulsar (HIPSR) system (Keith et al. 2010; Keane & Petroff 2015; Price et al. 2016). The BPSR produces 8-bit, Stokes-I filterbanks with spectral and temporal resolution of 390.625 kHz and 64 μs, respectively, over 1182–1152 MHz (340 MHz bandwidth). Searches for FRBs in the filterbanks were performed in real time using the dedicated GPU-based single pulse search software, HEIMDALL.[10] Candidate selection criteria are listed in section 3.3.2 of Keane et al. (2018). No FRBs were detected in real-time with S/N $\geq$ 10. A more thorough offline processing of the data with a lower S/N threshold of 6 did not yield any significant FRB detections either.

Molonglo – The Molonglo radio telescope, a Mills-cross design interferometer located near Canberra, Australia, is a pulsar timing and FRB detection facility (Bailes et al. 2017). Molonglo is sensitive to right-hand circularly polarized radiation, and operates in the spectral range of 820–850 MHz. The relatively large (≈ 4 deg $\times$ 2.8 deg) primary beam of Molonglo is tiled with 352 thin synthesized 'fanbeams' that overlap at their FWHM (≈ 45 arcsec). The output of each fanbeam is an 8-bit filterbank with spectral and temporal resolution of 98 kHz and 327 μs, respectively. These filterbanks were searched for FRBs using a modified version of

---

[7]https://heasarc.gsfc.nasa.gov/W3Browse/fermi/fermigbrst.html
[8]https://heasarc.gsfc.nasa.gov/W3Browse/fermi/fermigtrig.html
[9]https://gcn.gsfc.nasa.gov/fermi_gbm_subthresh_archive.html

[10]https://sourceforge.net/projects/heimdall-astro/
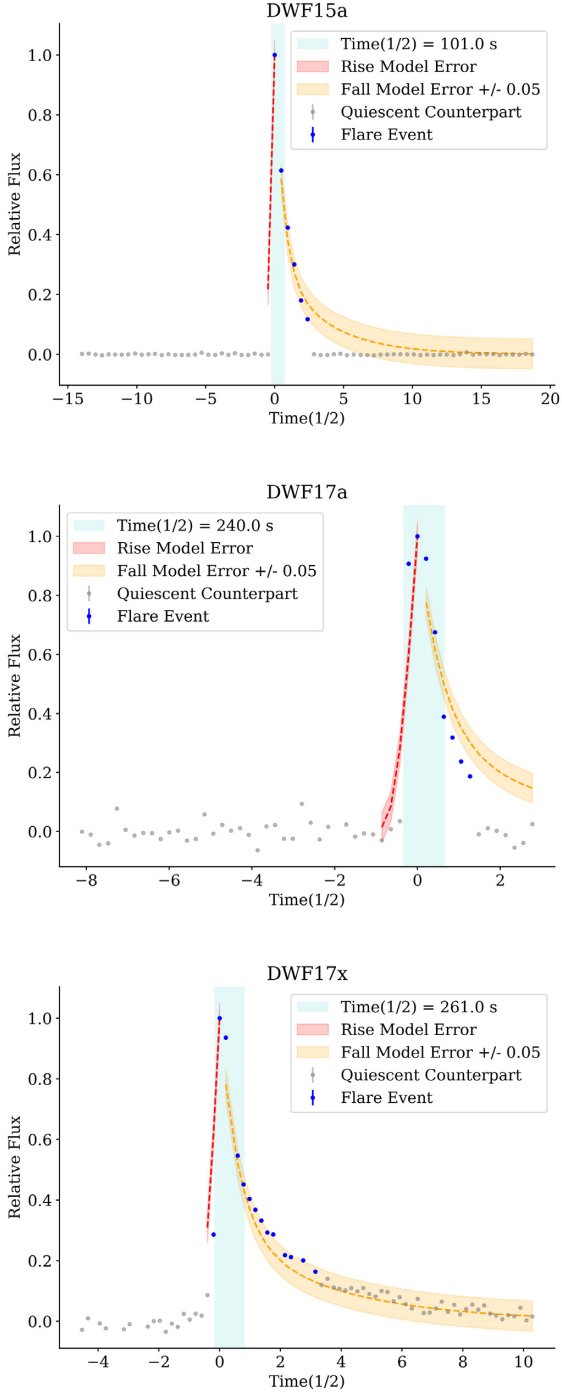
Figure 10. Flare-star model for the eFTC DWF15a (top), DWF17a (centre), and DWF17x (bottom). Data are compared with template white light flares based on *Kepler* observations (Davenport et al. 2014), where time(1/2) is the FWHM of the flare. When no permanent source is detectable in fast-cadenced *g*-band images outside the flare times, we simulate a Gaussian distribution of data points centred on the magnitude value (or upper limit) calculated on deep stacks (see Table 4). We normalized the flux to the brightest point of the light curve, however the peak of the flare is likely brighter and shifted in time by $0 \lesssim t_{\text{peak}} \lesssim 30$ s, given the cadence of our observations. A better guess of time and flux of the peak would likely result in a better fit of the model to the light curves in some cases, but poorer in others.

HEIMDALL, and burst candidates are validated via a machine learning pipeline operating in real-time (Farah et al. 2018, 2019). We searched for FRBs with widths in the range 327 µs to 42 ms, dispersion measures (DMs) in the range $0 < \text{DM} < 5000$ pc cm^{-3}.

Both Parkes and Molonglo were observing the region of sky where the selected eFTC were discovered, and the results are summarized in Table 6. No FRBs were detected during the observations.

5.3 Optical interleaved and long-term follow-up

We obtained photometry from the SkyMapper 1.35 m telescope located at Siding Spring Observatory in New South Wales, Australia (Keller et al. 2007). We have established a follow-up programme which coordinates with the DWF programme to obtain interleaved nightly observations during DWF (hours-later observations once it becomes night in Australia), and late-time regularly cadenced observations weeks after DWF to characterize long-duration transients and those that can be associated with fast transients, such as supernova shock breakouts. We obtained 100 s exposures in *gr* bands centred on each DWF field, which were covered by the wide-field of view of SkyMapper (5.7 deg^2) when weather is suitable. Whenever possible, we obtained template images prior to the DWF run. We used the SkyMapper Transient Survey Pipeline (Scalzo et al. 2017) to detect transients and obtain subtracted photometry. In addition to these images, we obtained photometry from the SkyMapper Supernova Survey (Scalzo et al. 2017) and the Southern Sky Survey (Wolf et al. 2018) when available for the candidates discussed in this work. These images were used to check for long-term variability and are available in the *uvgriz* passbands up to magnitudes $i = 20.27$, $z = 19.42$, $u = 19.34$, $v = 19.59$, $g = 21.57$, $r = 21.25$ depending on the coverage of the source. Long-term variability was verified from 2016 March to 2018 June for DWF17a, DWF17c, DWF17f, DWF17g and up to 2017 March for DWF17k, DWF17x and up to 2018 August for DWF17ao and DWF17ax (see Appendix, available online).

In this search for an optical counterpart to the fast transient candidates, there were no sources at the location of the DWF transients except for two cases, DWG17f and DWF17g. DWF17f was detected in the *z* filter on March 26th 2016 with magnitude 19.1 ± 0.1. DWF17g was detected more than once with SkyMapper in the *gr* bands on February 22 and 27 and *z* band on March 26 but we did not see any significant variability in any of the observations ($g = 21.0$, $r = 20.2$, $z = 19.1$).

6 RATES OF EXTRAGALACTIC FAST OPTICAL TRANSIENTS

Under the assumption that all the minute-time-scale transients that we detected are of Galactic nature, we can estimate upper limits to the rates for extragalactic fast optical transients. We follow the same procedure presented in Berger et al. (2013b) in order to enrich and extend the results that they obtained. The rate of extragalactic fast transients is defined as

$$R_{\text{eFT}} = N/(e_\tau * E_A), \tag{1}$$

where N is the number of transient events (here, $N = 3$ is defined for a non-detection, 95 per cent confidence), e_τ is the detection efficiency for the chosen time-scale, E_A is the effective areal exposure, defined as

$$E_A = \text{FoV}_{\text{eff}} * (n_{\text{im,tot}}/n_{\text{im,set}}) * \tau, \tag{2}$$

Table 6. This table indicates when gamma-ray and radio telescopes were observing the region of sky where a subset of eFTCs (Table 4) were discovered. The onset time indicated represents the MJD of the last non-detection of the eFTC. We looked into *Swift*/BAT data to identify gamma-ray counterparts, and we used the Parkes and Molonglo radio telescopes to search for FRBs. We coordinated *Swift*, Parkes, and Molonglo to observe fields simultaneously with DECam as part of the DWF programme. In addition, we looked for gamma-ray triggers issued by the *Fermi* satellite ± 1 d from the onset time, with the caveat that the location where the eFTC was detected may have been outside the *Fermi* field of view for part of the time.

ID	Onset (MJD)	*Fermi* (d)	*Swift*/BAT (min)	Parkes (min)	Molonglo (min)	Gamma-ray detections	FRB detections
DWF17k	57789.27229	$+/- 1$	$+8 +30$	$-5 +60$	$-8 +65$	0	0
DWF17x	57786.29119	$+/- 1$	$-10-3; +3 +27$	$-25 +45$	–	0	0
DWF17ao	57790.24767	$+/- 1$	–	$-45 +35$	$-2 +25$	0	0
DWF17ax	57789.24627	$+/- 1$	$-30-18$	$-20 +30$	$-47 +12$	0	0

where FoV_{eff} is the effective field of view explored, $n_{im, tot}$ is the total number of images, $n_{im, set}$ is the number of images constituting the smallest set that allows exploration of the chosen time-scale, and τ is the evolution time-scale of the transient. In this work, we analysed 25.76 h of data, over 10 half-nights. We searched for transients over an effective area of $\sim 2.52 \deg^2$ per pointing. The efficiency of the detection pipeline is based on the test results described in Andreoni et al. (2017), that returned 96.7 per cent completeness matching two consecutive epochs at S/N >10. Thus, we can assume $e_\tau = 0.967$ for the exploration of the shortest time-scale, where two (and only 2) detections must occur in consecutive images. The completeness rapidly reaches > 99.9 per cent for the exploration of longer time-scales thanks to the fact that a transient is selected even if 'missed' in $\sim 1/3$ of the images that lie between the first and the last detection of the event on the first night it was detected (with first and last images included in the count).

The shortest time-scale that we can explore is $\tau = 1.17$ min or 1 min 10 s, considering 20 s exposures interleaved by 30 s off-sky time. We obtain $E_A = 1.91 \deg^2$ d and an upper limit for the areal rate of $R_{eFT} < 1.625 \deg^{-2} d^{-1}$, represented with a yellow marker in Fig. 6. The results for every combination of time-scale and depth are plotted in Fig. 6 and presented in the Appendix (available online). Results of past surveys are summarized in Berger et al. (2013b) and include the Pan-STARRS1 Medium-Deep Survey (PS1/MDS Berger et al. 2013b), the Deep Lens Survey (DLS, Becker et al. 2004), the survey of the Fornax galaxy cluster (Rau et al. 2008), ROTSE III (Rykoff et al. 2005), and MASTER (Lipunov et al. 2007). In Fig. 6, we consider the case in which all the selected eFTCs are Galactic in nature or spurious detections.

7 DISCUSSION

This work probed the minute-time-scale transient sky with deep and fast-cadenced optical observations. Such a region of the time-scale-depth phase space is accessible with only a few existing facilities and no search with the combination of area, depth, and fast cadence of DWF has ever been performed. Our searches unveiled hundreds of transient and variable events, many of which evolve in minutes. Nine eFTC passed our specific extragalactic fast transient selection criteria, all of which are coincident with faint counterparts likely to be stellar.

Our selection criteria helped reduce contamination from Galactic sources and from transients (Galactic or extragalactic) evolving at time-scales longer than ~ 1 h. On the other hand, we are heavily biased towards discovering flare stars by imposing such strict temporal constraints. In particular, we expect to detect 'strong'

flares from distant ($\gtrsim 2$ kpc), late-type M-dwarfs difficult to detect when quiescent, as these would pass our non-stellar criteria for extragalactic events using our stellarity classifier. Our results (see Section 4) suggest those expectations to be correct, as most of the selected eFTCs are likely associated with late-type (usually $\geq$ M6) stars.

Although no deep spectra of the eFTCs exist, their peak and quiescent magnitudes and short evolution duration provide some limits on their nature when compared to known transients. The quiescent colours and magnitudes of DWF17k, DWF17x, DWF17ao, and DWF17ax are consistent (or roughly consistent) with an M9, M9/L, M5/M6, and M6 star at ~ 100, < 100, 1000–1500, and 850–1200 pc, respectively, and are thus thought to be flare stars. However, their star/galaxy classifications are less robust than for other candidates. If the quiescent objects were instead host galaxies, their colours are inconsistent with star-forming and other galaxy templates, but could be reddened elliptical or E + S0 galaxies, luminous infrared galaxies, or similar at $z \sim 0.5$–1.5, depending on galaxy type. The quiescent magnitudes are too bright for host galaxies at $z > 2$, placing them on the bright tip of the galaxy luminosity functions ($M \sim -23$ and brighter) before extinction correction.

If the eFTCs are considered as fast nova-like bursts ($M \sim -8$ to -9), their host galaxies are constrained to $M \sim -5$ to -9 compact dwarf galaxies or globular clusters at ~ 4–11 Mpc. If considered as supernova shock breakouts ($M \gtrsim -20$ adopted here), the hosts are constrained to $z < 0.25$–0.4 and the late-time photometric limits requires any associated supernova to fainter than $M \sim -14$ to -19 at ~ 100 Mpc to $z \sim 0.3$, respectively. The quiescent colours are inconsistent with essentially all galaxy types in this redshift range, unless heavily reddened. Finally, if the eFTCs are optical counterparts to GRBs, the quiescent colours and magnitudes are roughly consistent with $M \sim -21$ to -23 reddened host galaxies at $z \sim 0.5$–1.5 and optical afterglows of $M \sim -22$ to -23 before host or event extinction corrections.

During searches for extragalactic fast transients, hostless candidates may be excluded because their light curves resemble flare-star light curves. To test the validity of such an argument, we compared the template flare-star model (described in Section 4) with the light curve of the prompt optical flash that accompanied GRB 110205A at redshift $z = 2.22$ (Cucchiara et al. 2011). The flash remained visible for less than 15 min, providing a good example for the type of fast transient that this work targeted. Fig. 11 shows that, even without applying any re-scaling of the light curve at lower or higher redshift, the white light data points are consistent with the flare-star template. This comparison suggests that the lack of a bright host galaxy and light-curve information alone cannot exclude the extragalactic nature of a fast transient candidate.
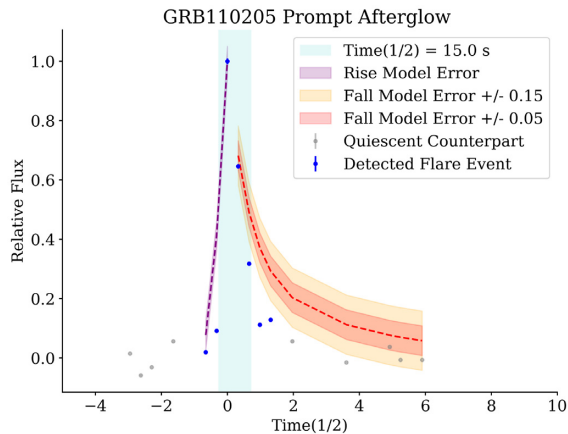
Figure 11. Observations of the optical flash associated with GRB110205A (Cucchiara et al. 2011) are compared with the Davenport et al. (2014) flare-star model described in Section 4 and Fig. 10.
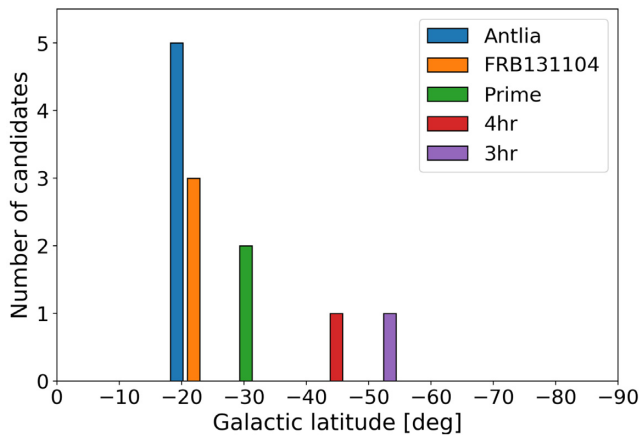

Figure 12. The number of eFTCs in Table 4 plotted against Galactic latitude, expressed in degrees. The bars of the histogram are 2° wide. The increase in the number of eFTCs in the Antlia field may be higher than expected as a result of the lower Galactic latitude (when extrapolating to zero latitude), or may indicate detection of extragalactic fast transients, given the proximity of the galaxy cluster. However, we caution that the sample is too small for any definitive result.

The distribution of eFTCs over Galactic latitude (Fig. 12) provides further indication that most of our eFTCs are Galactic flare stars, as they appear to be more common as the target fields approach the Galactic plane. A strong caveat is that Antlia is the field located at the lowest Galactic latitude among the fields considered in this analysis, but also includes the nearby Antlia galaxy cluster, which is at a comoving distance of ∼41 Mpc. Therefore, our observations cannot yet exclude that minute-time-scale fast optical transients are detectable with deep, fast-cadence observations both in our Galaxy and in the outskirts of nearby galaxies. The dependence of the number of eFTCs on Galactic latitude seems consistent with targeted flare-star population studies (e.g. West et al. 2008; Kowalski et al. 2009; Hilton et al. 2010; Chang, Wolf & Onken 2019). We refrain from further quantifying such dependence because of the small number of eFTCs reported in this paper, leaving it as the primary subject of a separate on-going analysis.

Finally, light curves of confirmed stellar flares show diverse behaviour, usually made more complex by a series of flares occurring in short time frames. High time sampling can help understand the

physics of flare stars and improve temporal morphology studies. Flaring events such as the double-peak event in Fig. 1 show that poor cadence can lead to misleading interpretation of parameters such as the flare duration, without accounting for the presence of multiple peaks. In addition, fit-to-peak estimates of peak luminosity and released energy can be overestimated using simple power-law fits. Such overestimation can affect the study of flares individually as well as a population, while underestimating the complexity of the flaring activity. Deep imaging and fast time sampling are necessary to compute quantities such as the duration and peak luminosity of the flares. Future work (Webb et al., in preparation) will include detailed and complete studies of hundreds of flare stars identified during the analysis presented in this work.

8 SUMMARY

In this paper, we analysed part of the all-wavelength and all-messenger DWF programme data set searching for extragalactic fast transients. Hundreds to thousands of astronomical transient and variable sources were discovered in DECam optical data, nine of which (see Table 4) passed strict selection criteria, described in Section 3.1. Those eFTCs (extragalactic fast transient candidates) are well constrained in time, within observing windows of ∼1 h, and appear not to be coincident with stellar sources. Adding optical multiband star/galaxy separation measurements to g-band information, we conclude that all the selected candidates are likely to have stellar progenitors. In addition, simultaneous (and near-simultaneous) multiwavelength observations did not identify FRBs using the Parkes and Molonglo radio telescopes, or gamma-ray events associated with those eFTCs using the *Swift* and *Fermi* satellites. Those eFTC showed no significant long-term variability detectable at approximate $i = 20.27$, $z = 19.42$, $u = 19.34$, $v = 19.59$, $g = 21.57$, $r = 21.25$ magnitude limits.

We have estimated areal rates of extragalactic fast transients at time-scales ranging between 1.17 and 52.0 min, between $23 \lesssim g \lesssim 24.7$ survey limiting magnitudes. We assumed that all our detections are Galactic flares, which is the most likely scenario, and we place rate upper limits (see the Appendix available online) in new regimes of the 'deep and fast' region of the phase space.

In large surveys focused on extragalactic astronomy, fast optical transients may be rejected as 'contaminant' stellar flares based on their light curve. However, we showed that light curves of confirmed extragalactic fast transients (such as the prompt optical flash of GRB110205A) can mimic the behaviour of Galactic flare-star light curves. This fact suggests that more solid criteria than 'hostless' and 'with flare-star-like light curve' should always be adopted when searching for extragalactic transients in optical surveys. Simultaneous multiwavelength and multimessenger observations, along with rapid detection and prompt or long-term follow-up is key to characterizing the fast transient sky. Future DWF programme observations can further improve our understanding of the minute-time-scale transient sky in the optical, as well as unveil the nature of the fastest bursts across several bands of the electromagnetic spectrum and using multiple messengers.

REFERENCES

Abbott B. et al., 2017, ApJ, 848, L12
Andreoni I., Cooke J., 2018, Proceedings of the International Astronomical Union, IAU Symposium, Vol. 339, Southern Horizons in Time-Domain Astronomy, p. 135
Andreoni I., Jacobs C., Hegarty S., Pritchard T., Cooke J., Ryder S., 2017, Publ. Astron. Soc. Aust., 34, e037
Annunziatella M., Mercurio A., Brescia M., Cavuoti S., Longo G., 2013, PASP, 125, 68
Arcavi I., 2018, ApJ, 855, L23
Arcavi I. et al., 2016, ApJ, 819, 35
Arcavi I. et al., 2017, Nature, 551, 64
Astier P. et al., 2006, A&A, 447, 31
Bailes M. et al., 2017, Publ. Astron. Soc. Aust., 34, e045
Barthelmy S. D. et al., 2005, Space Sci. Rev., 120, 143
Becker A. C. et al., 2004, ApJ, 611, 418
Bellm E. C. et al., 2019, PASP, 131, 018002
Berger E., Fong W., Chornock R., 2013a, ApJ, 774, L23
Berger E. et al., 2013b, ApJ, 779, 18
Bersten M. C. et al., 2018, Nature, 554, 497
Bertin E., Arnouts S., 2010, Astrophysics Source Code Library, record ascl:1010.064
Bleem L. E., Stalder B., Brodwin M., Busha M. T., Gladders M. D., High F. W., Rest A., Wechsler R. H., 2015, ApJS, 216, 20
Cenko S. B., 2017, Nat. Astron., 1, 0008
Cenko S. B. et al., 2015, ApJ, 803, L24
Chang S.-W., Wolf C., Onken C. A., 2019, MNRAS, 491, 39
Coulter D. A. et al., 2017, Science, 358, 1556
Cowperthwaite P. S. et al., 2017, ApJ, 848, L17
Cowperthwaite P. S. et al., 2018, ApJ, 858, 18
Cucchiara A. et al., 2011, ApJ, 743, 154
Dark Energy Survey Collaboration, 2016, MNRAS, 460, 1270
Davenport J. R. A. et al., 2014, ApJ, 797, 122
De K. et al., 2018, Science, 362, 201
Doctor Z. et al., 2017, ApJ, 837, 57
Drake A. J. et al., 2009, ApJ, 696, 870
Drout M. R. et al., 2014, ApJ, 794, 23
Farah W. et al., 2018, MNRAS, 478, 1209
Farah W. et al., 2019, MNRAS, 488, 2989
Flaugher B. et al., 2015, AJ, 150, 150
Förster F. et al., 2016, ApJ, 832, 155
Fox D. W. et al., 2003, ApJ, 586, L5
Gaia Collaboration, 2016, A&A, 595, A1
Gaia Collaboration, 2018, A&A, 616, A1
Gao H., Ding X., Wu X.-F., Dai Z.-G., Zhang B., 2015, ApJ, 807, 163
Garnavich P. M., Tucker B. E., Rest A., Shaya E. J., Olling R. P., Kasen D., Villar A., 2016, ApJ, 820, 23
Graham M. J. et al., 2019, PASP, 131, 078001

Hamuy M., Pinto P. A., 1999, AJ, 117, 1185
Hardy L. K. et al., 2017, MNRAS, 472, 2800
Henden A. A., Templeton M., Terrell D., Smith T. C., Levine S., Welch D., 2016, AAVSO, 40, 430
Hilton E. J., West A. A., Hawley S. L., Kowalski A. F., 2010, AJ, 140, 1402
Ho A. Y. Q. et al., 2018, ApJ, 854, L13
Holoien T. W.-S. et al., 2017, MNRAS, 471, 4966
Jin Z.-P., Li X., Cano Z., Covino S., Fan Y.-Z., Wei D.-M., 2015, ApJ, 811, L22
Jin Z.-P. et al., 2016, Nat. Commun., 7, 12898
Jin Z.-P., Covino S., Liao N.-H., Li X., D'Avanzo P., Fan Y.-Z., Wei D.-M., 2019, Nat. Astron., 461
Kasliwal M. M. et al., 2010, ApJ, 723, L98
Kasliwal M. M. et al., 2017, Science, 358, 1559
Keane E. F., Petroff E., 2015, MNRAS, 447, 2852
Keane E. F. et al., 2018, MNRAS, 473, 116
Keith M. J. et al., 2010, MNRAS, 409, 619
Keller S. C. et al., 2007, Publ. Astron. Soc. Aust., 24, 1
Kowalski A. F., Hawley S. L., Hilton E. J., Becker A. C., West A. A., Bochanski J. J., Sesar B., 2009, AJ, 138, 633
Lipunov V. M. et al., 2007, Astron. Rep., 51, 1004
Lipunov V. et al., 2017, ApJ, 850, L1
Lorimer D. R., Bailes M., McLaughlin M. A., Narkevic D. J., Crawford F., 2007, Science, 318, 777
LSST Science Collaboration, 2009, preprint (arXiv:0912.0201)
Martin-Carrillo A. et al., 2014, A&A, 567, A84
Meegan C. et al., 2009, ApJ, 702, 791
Perley D. A. et al., 2009, ApJ, 696, 1871
Poznanski D. et al., 2010, Science, 327, 58
Price D. C., Staveley-Smith L., Bailes M., Carretti E., Jameson A., Jones M. E., van Straten W., Schediwy S. W., 2016, J. Astron. Instrum., 5, 1641007
Pursiainen M. et al., 2018b, MNRAS, 481, 894
Rau A., Ofek E. O., Kulkarni S. R., Madore B. F., Pevunova O., Ajello M., 2008, ApJ, 682, 1205
Rau A. et al., 2009, PASP, 121, 1334
Rest A. et al., 2018, Nat. Astron., 2, 307
Rodney S. A. et al., 2018, Nat. Astron., 2, 324
Rubin A., Gal-Yam A., 2017, ApJ, 848, 8
Rykoff E. S. et al., 2005, ApJ, 631, 1032
Scalzo R. A. et al., 2017, Publ. Astron. Soc. Aust., 34, e030
Sevilla-Noarbe I. et al., 2018, MNRAS, 481, 5451
Shappee B. J. et al., 2014, ApJ, 788, 48
Shivvers I. et al., 2016, MNRAS, 461, 3057
Soares-Santos M. et al., 2017, ApJ, 848, L16
Sokołowski M., Małek K., Piotrowski L. W., Wrochna G., 2010, Adv. Astron., 2010, 463496
Staveley-Smith L. et al., 1996, Publ. Astron. Soc. Aust., 13, 243
Stubbs C. W., Doherty P., Cramer C., Narayan G., Brown Y. J., Lykke K. R., Woodward J. T., Tonry J. L., 2010, ApJS, 191, 376
Swaters R. A., Valdes F. G., 2007, in Shaw R. A., Hill F., Bell D. J., eds, ASP Conf. Ser. Vol. 376, Astronomical Data Analysis Software and Systems XVI. Astron. Soc. Pac., San Francisco, p. 269
Tanaka M. et al., 2016, ApJ, 819, 5
Tanvir N. R., Levan A. J., Fruchter A. S., Hjorth J., Hounsell R. A., Wiersema K., Tunnicliffe R. L., 2013, Nature, 500, 547
Tanvir N. R. et al., 2017, ApJ, 848, L27
Tendulkar S. P. et al., 2017, ApJ, 834, L7
Troja E. et al., 2017, Nature, 547, 425
Troja E. et al., 2018, Nat. Commun., 9, 4089
Valdes F. G., Swaters R. A., 2007, in Shaw R. A., Hill F., Bell D. J., eds, ASP Conf. Ser. Vol. 376, Astronomical Data Analysis Software and Systems XVI. Astron. Soc. Pac., San Francisco, p. 273
Valenti S. et al., 2017, ApJ, 848, L24
van Roestel J. et al., 2019, MNRAS, 484, 4507
Vestrand W. T. et al., 2014, Science, 343, 38
Villar V. A. et al., 2017, ApJ, 851, L21
West A. A., Hawley S. L., Bochanski J. J., Covey K. R., Reid I. N., Dhital S., Hilton E. J., Masuda M., 2008, AJ, 135, 785
West A. A. et al., 2011, AJ, 141, 97
Wolf C. et al., 2018, Publ. Astron. Soc. Aust., 35, e010

SUPPORTING INFORMATION

Supplementary data are available at *MNRAS* online.

APPENDIX A. Upper limits for areal ratES

APPENDIX B. Skymapper photometry

Please note: Oxford University Press is not responsible for the content or functionality of any supporting materials supplied by the authors. Any queries (other than missing material) should be directed to the corresponding author for the article.

[1] *Swinburne University of Technology, PO Box 218, Hawthorn, VIC 3122, Australia*
[2] *Australian Astronomical Observatory, 105 Delhi Rd, North Ryde, NSW 2113, Australia*
[3] *ARC Centre of Excellence for Gravitational Wave Discovery (OzGrav), Swinburne University of Technology, PO Box 218, Hawthorn, VIC 3122, Australia*
[4] *Division of Physics, Math and Astronomy, California Institute of Technology, Pasadena, CA 91125, USA*
[5] *ARC Centre of Excellence for All-sky Astrophysics (CAASTRO), Building A28, School of Physics, The University of Sydney, Sydney, NSW 2006, Australia*
[6] *Space Telescope Science Institute, 3700 San Martin Dr., Baltimore, MD 21218, USA*
[7] *Department of Physics and Astronomy, Johns Hopkins University, 3400 North Charles Street, Baltimore, MD 21218, USA*
[8] *Center for Cosmology and Particle Physics, New York University, 726 Broadway, New York, NY 10004, USA*
[9] *Research School of Astronomy and Astrophysics, Australian National University, Canberra, ACT 2611, Australia*
[10] *Jodrell Bank Centre for Astrophysics, School of Physics and Astronomy, The University of Manchester, Manchester M13 9PL, UK*
[11] *Center for Research and Exploration in Space Science and Technology (CRESST) and NASA Goddard Space Flight Center, Greenbelt, MD 20771, USA*
[12] *Department of Physics, University of Maryland, Baltimore County, 1000 Hilltop Circle, Baltimore, MD 21250, USA*
[13] *Dipartimento di Fisica U2, Università degli Studi di Milano-Bicocca, Piazza della Scienza 3, Milano I-20126, Italy*
[14] *INAF – Osservatorio Astronomico di Brera, via Bianchi 46, Merate I-23807, Italy*
[15] *Cerro Tololo Inter-American Observatory, National Optical Astronomy Observatory, Casilla 603, 1700000 La Serena, Chile*
[16] *CSIRO Astronomy and Space Science, Australia Telescope National Facility, PO Box 76, Epping, NSW 1710, Australia*
[17] *College of Science and Mathematics, University of the Virgin Islands, #2 Brewers Bay Road, Charlotte Amalie 00802, USVI*
[18] *SKA Organisation, Jodrell Bank Observatory, Macclesfield SK11 9DL, UK*
[19] *Division of Theoretical Astronomy, National Astronomical Observatory of Japan, National Institutes of Natural Sciences, 2-21-1 Osawa, Mitaka, Tokyo 181-8588, Japan*
[20] *Department of Astronomy, University of California Berkeley, Berkeley, CA 94720, USA*
[21] *Anton Pannekoek Institute for Astronomy, University of Amsterdam, 1098 XH, Amsterdam, the Netherlands*
[22] *ASTRON, Netherlands Institute for Radio Astronomy, 7991 PD Dwingeloo, the Netherlands*
[23] *Department of Physics & Astronomy, Macquarie University, Macquarie Park, NSW 2109, Australia*

This paper has been typeset from a T_EX/L^AT_EX file prepared by the author.